



Eidgenössische Technische Hochschule Zürich  
Swiss Federal Institute of Technology Zurich

# Chiral $p$ -Wave Superconductivity Around Disclinations

Semester Thesis

Isidor Schoch

[isschoch@student.ethz.ch](mailto:isschoch@student.ethz.ch)

Condensed Matter Theory Group

Department of Physics

UZH

## Supervisors:

Professor Titus Neupert

Professor Manfred Sigrist

Martina Soldini

April 26, 2022

I would like to thank both Professor Sigrist and Professor Neupert for giving me the opportunity to do a project on chiral  $p$ -wave superconductivity. With this project, I was able to get a small glimpse of the vast and important field of condensed matter physics. Furthermore, I had the pleasure of working with my supervisor Martina Soldini who helped extensively throughout the project.

# Contents

<b>Acknowledgements</b>	<b>ii</b>
<b>1 Introduction</b>	<b>1</b>
<b>2 Theory</b>	<b>2</b>
2.1 Introduction to BCS Theory of Superconductivity . . . . .	2
2.2 Chiral $p$ -Wave Superconductivity . . . . .	4
2.3 Majorana Zero Modes . . . . .	5
<b>3 Results</b>	<b>8</b>
3.1 Vortex in a Square Lattice . . . . .	8
3.2 Square Lattice with a Single Disclination . . . . .	11
3.3 Square Lattice with Disclination Dipole . . . . .	13
3.4 Numerical Implementation . . . . .	15
<b>4 Conclusion</b>	<b>16</b>
4.1 Summary of the Project . . . . .	16
4.2 Outlook . . . . .	16

# Introduction

---

Superconductors are probably best known for their vanishing resistance in the superconducting phase. An arguably more important property of superconductors is the *Meissner effect*. The *Meissner effect* is the property of superconductors to become perfect diamagnets, i.e. they expel magnetic fields from their bulk [1]. Superconductivity arises due to the formation of Cooper-pairs which follow a *Bose-Einstein distribution*. Consequently, the pairs can form a condensate which is a superfluid [2]. In this thesis, we focus on chiral  $p$ -wave superconductivity in which the Cooper-pairs have a finite angular momentum. This can lead to a trapped magnetic flux around topological defects [3] in the lattice which counteracts the *Meissner effect*. Furthermore, it has been proposed that curved surfaces of Chiral  $p$ -wave superconductors can generate magnetic fields [4]. This effect is termed the *geometric Meissner effect*. In this semester thesis, the first steps towards studying the interplay between the *geometric Meissner effect* and the trapped magnetic flux around topological defects are made. One possible way of doing this is by simulating chiral  $p$ -wave superconductivity on a Buckyball geometry as the two effects are present. The Buckyball geometry is shown in figure 1.1. It consists of pentagons and hexagons. We can view the pentagons as topological defects in a hexagonal honeycomb lattice. Furthermore, such topological defects can give rise to so-called *Majorana zero modes* [3, 6, 7]. Such states could potentially be a break-through leading to fault-tolerant quantum computing [8].

We first revise the theoretical framework needed to describe chiral  $p$ -wave superconductors in chapter 2. In chapter 3 simulations on lattices with topological defects on a square lattice are performed and discussed. The final chapter 4 consists of a brief revision of the work done in this semester project and also mentions the next steps that are required to perform the full simulation on a Buckyball geometry.

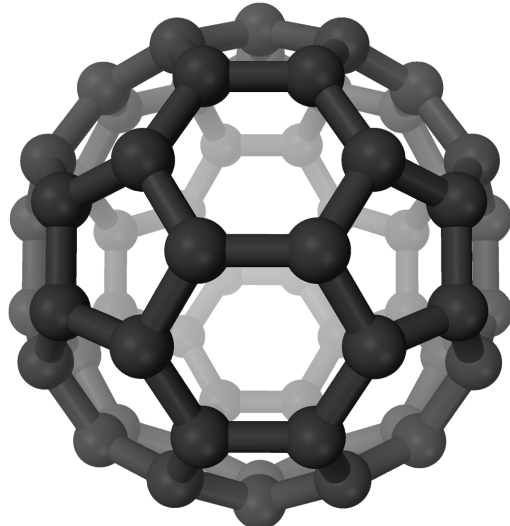


Figure 1.1: Buckyball Geometry [5]

# Theory

---

In order to describe chiral  $p$ -wave superconductors, we first investigate a simple model, the tight-binding model. This model allows us to describe non-interacting electrons hopping from atom to atom. Quite astonishingly, this simple model is nearly sufficient to describe a rather complex phenomenon that has been at the center of condensed matter physics research for nearly half a decade: A simple extension of the model leads to the most well-known form of superconductivity, so-called Singlet  $s$ -wave superconductivity. This type of model is coined after the initiators of the model as the Bardeen–Cooper–Schrieffer (BCS) theory of superconductivity. An additional simple extension of BCS theory allows us to also capture unconventional superconductivity. We can describe chiral  $p$ -wave superconductivity in this model. This first step allows us to investigate the phenomenon on different lattices, whereby lattices with different topological defects are of particular interest to us.

## 2.1 Introduction to BCS Theory of Superconductivity

We consider a Bravais lattice defined by the points  $\mathbf{r}_{n,m} = n\mathbf{a}_1 + m\mathbf{a}_2$  where  $\mathbf{a}_i \in \mathbb{R}^2$  are the lattice vectors and  $n, m \in \mathbb{Z}$  are arbitrary integers. For the sake of notational brevity, we often suppress the indices and therefore refer to a lattice point simply as  $\mathbf{r}$ . The reciprocal lattice vectors  $\mathbf{b}_j$  and the corresponding reciprocal lattice can be determined by the relation  $\mathbf{a}_i \cdot \mathbf{b}_j = 2\pi\delta_{ij}$ . First, we describe a material before it has undergone the superconducting transition, which we call the *normal state*, with a tight-binding model. The tight-binding model is described by the Hamiltonian

$$\mathcal{H}_{\text{TB}} = \sum_{\mathbf{r}} \varepsilon_{\mathbf{r}} \hat{c}_{\mathbf{r}}^\dagger \hat{c}_{\mathbf{r}} + \sum_{\mathbf{r} \neq \mathbf{r}'} t_{\mathbf{r}\mathbf{r}'} \hat{c}_{\mathbf{r}}^\dagger \hat{c}_{\mathbf{r}'} \quad (2.1)$$

in the second quantization formalism and can be used to describe non-interacting electrons traversing a lattice [9]. The operators  $\hat{c}_{\mathbf{r}}^{(\dagger)}$  are the fermionic annihilation (creation) operators on site  $\mathbf{r}$  and obey the commutation relations

$$\{\hat{c}_{\mathbf{r}}^\dagger, \hat{c}_{\mathbf{r}'}\} = \delta_{\mathbf{r}\mathbf{r}'} \quad \{\hat{c}_{\mathbf{r}}^\dagger, \hat{c}_{\mathbf{r}'}^\dagger\} = \{\hat{c}_{\mathbf{r}}, \hat{c}_{\mathbf{r}'}\} = 0 \quad (2.2)$$

which encode the Pauli-principle.

## 2 Theory

The probability of tunneling from site  $\mathbf{r}$  to site  $\mathbf{r}'$  is described by  $t_{\mathbf{r}\mathbf{r}'}$ . The potential energy is given by the first term and is associated with the on-site energy  $\varepsilon_{\mathbf{r}}$  on lattice site  $\mathbf{r}$ . For our purposes, we usually set the on-site energy to the negative chemical potential  $\varepsilon_{\mathbf{r}} = -\mu$ . One can calculate the band structure of the system by going to momentum space.

A common approximation used in tight-binding models is to only consider nearest neighbor (n. n.) interactions, which on a  $n \times n$  square lattice leads a Hamiltonian of the following form

$$\mathcal{H}_{\text{TB}} = \sum_{\mathbf{r}} -t(\hat{c}_{\mathbf{r}+\mathbf{a}_1}^\dagger \hat{c}_{\mathbf{r}} + \hat{c}_{\mathbf{r}-\mathbf{a}_1}^\dagger \hat{c}_{\mathbf{r}} + \hat{c}_{\mathbf{r}+\mathbf{a}_2}^\dagger \hat{c}_{\mathbf{r}} + \hat{c}_{\mathbf{r}-\mathbf{a}_2}^\dagger \hat{c}_{\mathbf{r}}) - \mu \hat{c}_{\mathbf{r}}^\dagger \hat{c}_{\mathbf{r}} \quad (2.3)$$

where  $t_{\mathbf{r}\mathbf{r}'} = -t$  for  $\mathbf{r}$  n. n. of  $\mathbf{r}'$  [9]. From now on we set the lattice vectors to be the standard basis vectors, i.e.  $\mathbf{a}_1 = \hat{\mathbf{x}}$  and  $\mathbf{a}_2 = \hat{\mathbf{y}}$ . The total number of sites for a finite lattice is denoted by  $N$ . We introduce the Fourier transform relations

$$\hat{c}_{\mathbf{k}} = \frac{1}{\sqrt{N}} \sum_{\mathbf{r}} \hat{c}_{\mathbf{r}} e^{-i\mathbf{k}\cdot\mathbf{r}} \quad \hat{c}_{\mathbf{r}} = \frac{1}{\sqrt{N}} \sum_{\mathbf{k}} \hat{c}_{\mathbf{k}} e^{i\mathbf{k}\cdot\mathbf{r}} \quad (2.4)$$

which allows us to switch between real and momentum space. Going to momentum space, using equation 2.4, we get the following Hamiltonian.

$$\mathcal{H}_{\text{TB}} = \sum_{\mathbf{k}} -2t(\cos(k_x) + \cos(k_y)) \hat{c}_{\mathbf{k}}^\dagger \hat{c}_{\mathbf{k}} - \mu \hat{c}_{\mathbf{k}}^\dagger \hat{c}_{\mathbf{k}} \quad (2.5)$$

In BCS theory of superconductivity so-called Cooper-pairs - pairs of electrons with opposite spin paired together through an attractive force which is mediated by phonons in the lattice structure - follow *Bose-Einstein statistics* and can therefore form a condensate [10, 11]. These interactions are dominated by terms with vanishing total momentum. After applying a *mean-field approximation* can write the BCS Hamiltonian as

$$\mathcal{H}_{\text{BCS}} = \mathcal{H}_{\text{TB}} + \sum_{\mathbf{k}} \Delta \hat{c}_{\mathbf{k}}^\dagger \hat{c}_{-\mathbf{k}}^\dagger + \Delta^* \hat{c}_{-\mathbf{k}} \hat{c}_{\mathbf{k}} = \sum_{\mathbf{k}} \Psi_{\mathbf{k}}^\dagger \begin{bmatrix} \frac{1}{2}\varepsilon_{\mathbf{k}} & \Delta \\ \Delta^* & -\frac{1}{2}\varepsilon_{-\mathbf{k}}^* \end{bmatrix} \Psi_{\mathbf{k}} + C \quad (2.6)$$

where  $\Psi_{\mathbf{k}}^\dagger = [\hat{c}_{\mathbf{k}} \quad \hat{c}_{-\mathbf{k}}^\dagger]^\dagger$  and  $\varepsilon_{\mathbf{k}} = -2t(\cos(k_x) + \cos(k_y)) - \mu$ . The constant  $C$  can be dropped as it does not influence the dynamics of the system. In this formulation, it is implied that the spin component of the Cooper-pair wave-function is in a *singlet* state. This is also, in turn, what allowed us to describe *spin-singlet s-wave* superconductivity as a spin-less system. To describe lower symmetry states, such as *spin-triplet* states, we include the spin system in the Hamiltonian from now on.

## 2 Theory

### 2.2 Chiral $p$ -Wave Superconductivity

Chiral  $p$ -wave superconductivity is characterized by the Cooper-pair having angular momentum  $l = 1$ . As a direct consequence, the state is time-reversal symmetry breaking. This is in contrast to the highest symmetry *spin-singlet*  $s$ -wave state covered in the previous chapter. One of the distinctions between conventional and unconventional superconductivity is that the gap function  $\Delta$  can be momentum dependent in the latter case. In the spin subspace  $\text{span}\{|\uparrow\rangle, |\downarrow\rangle\}$  the gap function for a  $p$ -wave superconductor is

$$\hat{\Delta}(\mathbf{k}) = \begin{bmatrix} 0 & \frac{\Delta}{k_F}(\sin(k_x) \pm i \sin(k_y)) \\ \frac{\Delta}{k_F}(\sin(k_x) \pm i \sin(k_y)) & 0 \end{bmatrix} = i(\mathbf{d}_\mathbf{k} \cdot \boldsymbol{\sigma})\sigma_y \quad (2.7)$$

where  $\mathbf{d}_\mathbf{k} = \frac{\Delta}{k_F}(\sin(k_x) \pm i \sin(k_y))\hat{\mathbf{z}}$  is the  $\mathbf{d}$ -vector [11]. In combination with the so-called Bloch-Hamiltonian

$$H(\mathbf{k}) = \begin{bmatrix} \frac{1}{2}\varepsilon_\mathbf{k} & 0 \\ 0 & \frac{1}{2}\varepsilon_\mathbf{k} \end{bmatrix} \quad (2.8)$$

again represented acting on the spin system we can construct the complete Hamiltonian in Nambu space

$$\mathcal{H}_{p\text{-wave}} = \sum_{\mathbf{k}} \Psi_{\mathbf{k}}^\dagger H_{\text{BdG}}(\mathbf{k}) \Psi_{\mathbf{k}} \quad (2.9)$$

where we define the Nambu basis spinor  $\Psi_{\mathbf{k}}^\dagger = [\hat{c}_{\mathbf{k}\uparrow} \quad \hat{c}_{\mathbf{k}\downarrow} \quad \hat{c}_{-\mathbf{k}\uparrow}^\dagger \quad \hat{c}_{-\mathbf{k}\downarrow}^\dagger]^\dagger$  [11, 12]. The matrix between the two spinors is the Bogolyubov-de-Gennes Hamiltonian [12].

$$H_{\text{BdG}} = \begin{bmatrix} H(\mathbf{k}) & \hat{\Delta}(\mathbf{k}) \\ \hat{\Delta}(\mathbf{k})^\dagger & -H(-\mathbf{k})^* \end{bmatrix} \quad (2.10)$$

This Hamiltonian has *particle hole-symmetry* which can be confirmed by calculating the anti-commutation relation between the particle-hole exchange operator  $\mathcal{P} = (\sigma_x \otimes \mathbb{1})\mathcal{K}$  and the Hamiltonian.

$$\mathcal{P}H_{\text{BdG}}\mathcal{P}^{-1} = -H_{\text{BdG}} \quad (2.11)$$

We can also describe chiral  $p$ -wave superconductivity in real space by using the Fourier transform relations 2.4. This results in the following representation of the Hamiltonian.

$$\mathcal{H}_{p\text{-wave}} = \sum_{\mathbf{r}\sigma} -\mu \hat{c}_{\mathbf{r},\sigma}^\dagger \hat{c}_{\mathbf{r}\sigma} - t(\hat{c}_{\mathbf{r}+\hat{\mathbf{x}}\sigma}^\dagger \hat{c}_{\mathbf{r}\sigma} + \hat{c}_{\mathbf{r}-\hat{\mathbf{x}}\sigma}^\dagger \hat{c}_{\mathbf{r}\sigma} + \hat{c}_{\mathbf{r}+\hat{\mathbf{y}}\sigma}^\dagger \hat{c}_{\mathbf{r}\sigma} + \hat{c}_{\mathbf{r}-\hat{\mathbf{y}}\sigma}^\dagger \hat{c}_{\mathbf{r}\sigma}) \quad (2.12)$$

$$+ \frac{1}{2}\Delta(\hat{c}_{\mathbf{r}+\hat{\mathbf{y}}\sigma}^\dagger \hat{c}_{\mathbf{r}-\sigma}^\dagger - \hat{c}_{\mathbf{r}-\hat{\mathbf{y}}\sigma}^\dagger \hat{c}_{\mathbf{r}-\sigma}^\dagger - i(\hat{c}_{\mathbf{r}+\hat{\mathbf{x}}\sigma}^\dagger \hat{c}_{\mathbf{r}-\sigma}^\dagger - \hat{c}_{\mathbf{r}-\hat{\mathbf{x}}\sigma}^\dagger \hat{c}_{\mathbf{r}-\sigma}^\dagger)) + \text{h.c.} \quad (2.13)$$

## 2 Theory

If we introduce a spinor in real space  $\Psi_{\mathbf{r}}^\dagger = [\hat{c}_{\mathbf{r}_1,1\uparrow} \quad \hat{c}_{\mathbf{r}_1,1\downarrow} \quad \hat{c}_{\mathbf{r}_1,1\uparrow}^\dagger \quad \hat{c}_{\mathbf{r}_1,1\downarrow}^\dagger \quad \hat{c}_{\mathbf{r}_1,2\uparrow} \quad \dots \quad \hat{c}_{\mathbf{r}_n,n\downarrow}^\dagger]^\dagger$  we can write the Hamiltonian as

$$\mathcal{H}_{p\text{-wave}} = \Psi_{\mathbf{r}}^\dagger H_{\mathbf{r}} \Psi_{\mathbf{r}} \quad (2.14)$$

where  $H_{\mathbf{r}}$  consists of blocks for which we only have to distinguish between three different cases: The on-site block, a hopping block along  $\hat{\mathbf{x}}$ , and a hopping block along  $\hat{\mathbf{y}}$ .

$$H_{\mathbf{r}_{i,j} \rightarrow \mathbf{r}_{i,j}} = \frac{1}{2} \begin{bmatrix} -\mu\sigma_0 & 0 \\ 0 & \mu\sigma_0 \end{bmatrix} \quad (2.15)$$

$$H_{\mathbf{r}_{i,j} \rightarrow \mathbf{r}_{i,j} \pm \hat{\mathbf{x}}} = \frac{1}{2} \begin{bmatrix} -t\sigma_0 & \pm i\Delta\sigma_x \\ \pm i\Delta\sigma_x & t\sigma_0 \end{bmatrix} \quad (2.16)$$

$$H_{\mathbf{r}_{i,j} \rightarrow \mathbf{r}_{i,j} \pm \hat{\mathbf{y}}} = \frac{1}{2} \begin{bmatrix} -t\sigma_0 & \mp \Delta\sigma_x \\ \pm \Delta\sigma_x & t\sigma_0 \end{bmatrix} \quad (2.17)$$

$$H_{\mathbf{r}} = \begin{bmatrix} H_{\mathbf{r}_{0,0} \rightarrow \mathbf{r}_{0,0}} & H_{\mathbf{r}_{0,0} \rightarrow \mathbf{r}_{0,1}} & 0 & \cdots & H_{\mathbf{r}_{0,0} \rightarrow \mathbf{r}_{1,0}} & \cdots \\ H_{\mathbf{r}_{0,1} \rightarrow \mathbf{r}_{0,0}} & H_{\mathbf{r}_{0,1} \rightarrow \mathbf{r}_{0,1}} & H_{\mathbf{r}_{0,1} \rightarrow \mathbf{r}_{0,2}} & \cdots & H_{\mathbf{r}_{0,1} \rightarrow \mathbf{r}_{1,1}} & \cdots \\ \vdots & \ddots & & & & \\ & & & & & \\ & & & & & H_{\mathbf{r}_{n,n} \rightarrow \mathbf{r}_{n,n}} \end{bmatrix} \quad (2.18)$$

### 2.3 Majorana Zero Modes

*Majorana zero modes* are zero-energy quasiparticle states and are characterized by their non-locality, which makes them resistant to decoherence [8]. The non-locality of the state is often manifested as the wave-function having its support exponentially localized on the edges or around topological defects of the lattice [13]. We consider p-wave superconductivity on finite-size systems with open boundary conditions. According to the *bulk-edge correspondence*, different topological phases are protected as long as there is a gap in the band structure of the bulk [14]. We calculate the bulk band structure by diagonalizing  $H_{\text{BdG}}$  of equation 2.10 and get the following spectrum for a 2D infinite square lattice.

$$E^\pm(\mathbf{k}) = \pm \sqrt{(t(\cos(k_x) + \cos(k_y)) + \mu/2)^2 + |\Delta|^2(\sin(k_x)^2 + \sin(k_y)^2)} \quad (2.19)$$

We may ignore the spin-degeneracy and focus on calculating for which parameter values the upper  $E^+$  and lower  $E^-$  bands touch and hence close the superconducting gap. One can heuristically argue that crossing these critical points corresponds to transitions between phases where topologically protected *Majorana states* are present or not [15]. To simplify the analysis, we set  $t/|\Delta| = 1$ .

## 2 Theory

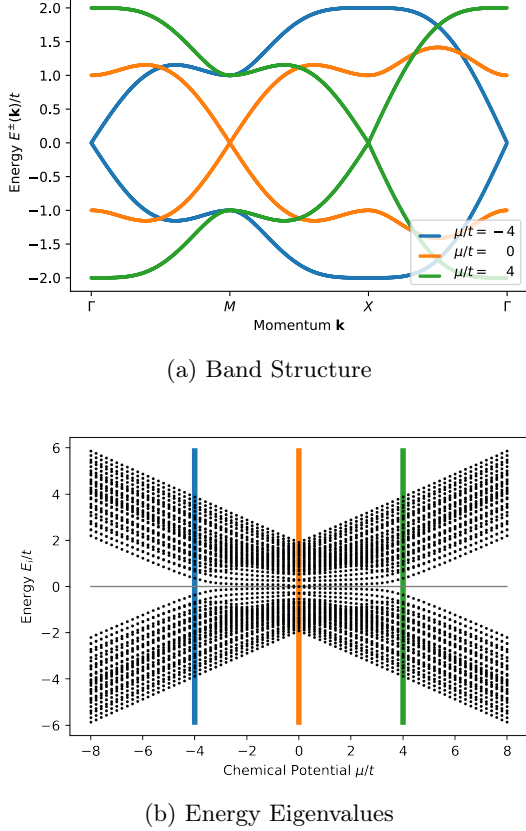


Figure 2.1: Topological Phases of Chiral  $p$ -wave superconductivity on Square Lattice

both the bulk and the straight edges. The probability distribution in figure 2.3b corresponds to the state with the lowest absolute energy. The spectrum is shown in figure 2.2a. As a consistency check, we can take a finite square lattice with periodic boundary conditions. The periodic boundary conditions remove edges in the lattice and can be implemented by adding a bond between edge lattice sites on opposite sides of the lattice. We would not expect such a system to exhibit *Majorana modes*. This is indeed the case as can be seen in figure 2.3. Note that the state with the lowest absolute value of energy was used to plot the probability distribution shown in figure 2.3b.

We find that for  $\mathbf{k} = \mathbf{0}$  and  $\mu/t = -4$  the superconducting gap vanishes. When  $\mu/t = 4$  we get the same result at  $\mathbf{k} = \pi(\hat{\mathbf{x}} + \hat{\mathbf{y}})$ . The last critical value can be found at  $\mathbf{k} = \pi\hat{\mathbf{x}}$  for  $\mu = 0$ . An overview of the bulk band structure for different  $\mu$  is shown in figure 2.1a. By analyzing the spectrum for different ratios of  $\mu/t$  we can find out which phases contain zero modes in their spectrum. The phases with *Majorana modes* lie in the range  $\mu/t \in (-4, 4)$  as shown in figure 2.1b. If one wants to rigorously prove the existence of the topological phase one must calculate the appropriate topological invariant, such as the chiral winding number or the Wilson loop [16]. As this goes beyond the scope of this project we leave this to [12].

With the theoretical groundwork established we should now be able to observe *Majorana states* if we choose the appropriate parameters. As an example, such a *Majorana state* is depicted in figure 2.2b for a square lattice and  $\mu/t = 2\Delta/t = 2$ . As expected we see that the state is strongly localized around the corners and edges of the system. The corners of the system have a particularly high probability density since they have the fewest neighbors which makes them distinct from

## 2 Theory

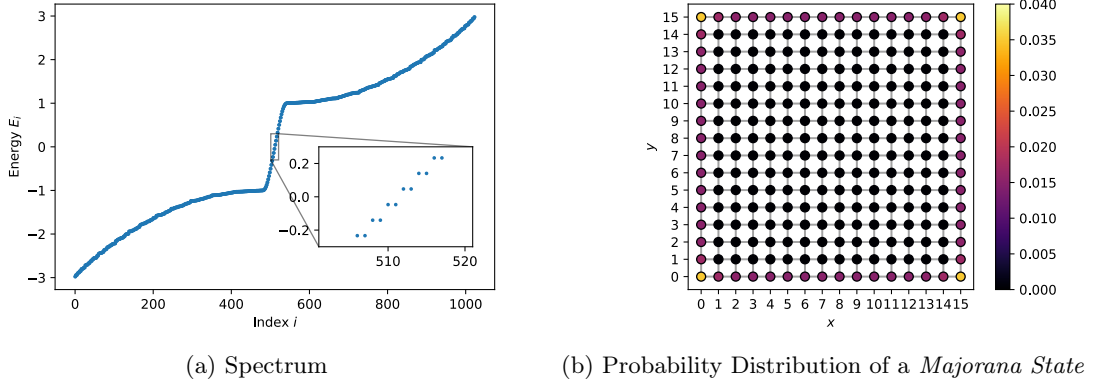


Figure 2.2: Chiral  $p$ -wave superconductivity on a Square Lattice with Open Boundary Conditions

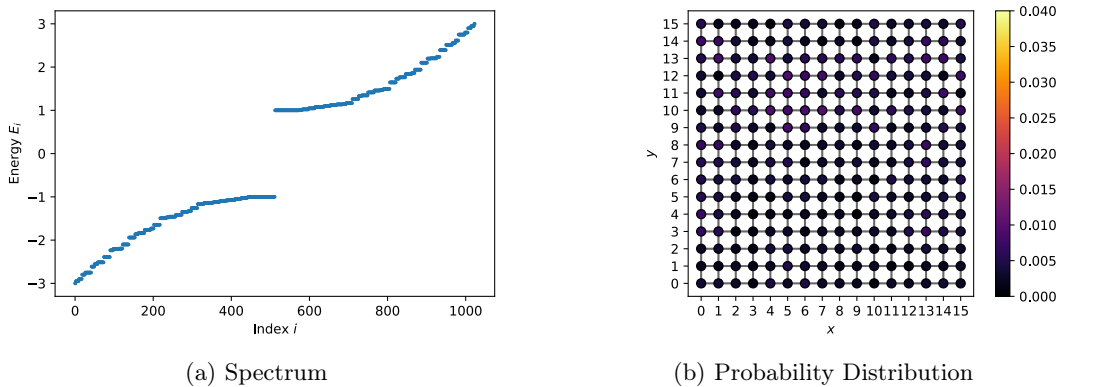


Figure 2.3: Chiral  $p$ -wave superconductivity on a Square Lattice with Periodic Boundary Conditions

# Results

---

In this chapter, we first investigate the formation of vortices in a square lattice. After this, we discuss how to treat disclinations that break rotational lattice symmetries. We then combine these defects with vortices centred around these disclinations and conclude the chapter by investigating a disclination dipole.

## 3.1 Vortex in a Square Lattice

So far we have seen that *Majorana zero modes* can form around the edges of the lattice. However, they can also be observed around vortices [3, 6]. A vortex is characterized by a Cooper-pair condensate depletion around a vortex core. The *de Broglie condition* around the vortex core leads to

$$\oint \nabla\phi(\mathbf{r}) \cdot d\mathbf{r} = 2\pi n_\phi \quad (3.1)$$

where  $n_\phi$  is the winding number and  $\phi$  is the phase of the condensate [17]. Certain winding numbers  $n_\phi$  classify as topological defects in the lattice which means that they cannot be created or destroyed. Using the London equations, one can calculate an associated magnetic flux of  $\pm\Phi_0/4$  to a vortex, meaning that a vortex traps a magnetic flux [3].

We can add a vortex by introducing a vortex phase of  $\phi_v = \pi$  to the creation and annihilation operators which cross certain bonds of the lattice [3, 7]. We have to choose these bonds such that any single path integral around a closed curve contains the vortex phase  $\phi_v$ . Thus, for any bonds between sites  $\mathbf{r}$  and  $\mathbf{r}'$  to which we wish to add a phase, we must apply the following transformations to the fermionic creation and annihilation operators.

$$\hat{c}_{\mathbf{r}'}^\dagger \hat{c}_\mathbf{r} \mapsto \hat{c}_{\mathbf{r}'}^\dagger \hat{c}_\mathbf{r} e^{i\phi_v} \quad (3.2)$$

$$\hat{c}_{\mathbf{r}'}^\dagger \hat{c}_\mathbf{r}^\dagger \mapsto \hat{c}_{\mathbf{r}'}^\dagger \hat{c}_\mathbf{r}^\dagger e^{i\phi_v} \quad (3.3)$$

$$\hat{c}_{\mathbf{r}'} \hat{c}_\mathbf{r}^\dagger \mapsto \hat{c}_{\mathbf{r}'} \hat{c}_\mathbf{r}^\dagger e^{-i\phi_v} \quad (3.4)$$

$$\hat{c}_{\mathbf{r}'} \hat{c}_\mathbf{r} \mapsto \hat{c}_{\mathbf{r}'} \hat{c}_\mathbf{r} e^{-i\phi_v} \quad (3.5)$$

Numerically, it is more convenient to absorb the phase factor into the block of  $H_{\mathbf{r}}$  associated with the bond.

### 3 Results

For example, say we want to add a phase to a bond along the  $\hat{\mathbf{x}}$ -direction. This can be achieved by transforming the block

$$H_{\mathbf{r}_{i,j} \rightarrow \mathbf{r}_{i,j} \pm \hat{\mathbf{x}}} = \frac{1}{2} \begin{bmatrix} -t\sigma_0 & \pm i\Delta\sigma_x \\ \pm i\Delta\sigma_x & t\sigma_0 \end{bmatrix} \mapsto \frac{1}{2} \begin{bmatrix} -t\sigma_0 e^{i\phi_v} & \pm i\Delta\sigma_x e^{i\phi_v} \\ \pm i\Delta\sigma_x e^{-i\phi_v} & t\sigma_0 e^{-i\phi_v} \end{bmatrix} \quad (3.6)$$

and the Hermitian conjugate for the reverse process [7]. Adding a phase along a  $\hat{\mathbf{y}}$ -bond is handled analogously. Such a vortex was implemented on a square lattice by adding a  $\phi_v = \pi$  phase to the bonds in the  $\hat{\mathbf{x}}$ -direction from the top edge to the middle of the lattice as indicated by the green arrows in figure 3.1b. The direction of the arrow signifies to which process the transformation 3.6 was applied. The reverse process with the Hermitian conjugate transformation is applied antiparallel to the arrow. As predicted in [3] we observe extremely well-defined zero-energy states on the order of  $E_i/t \sim 10^{-7}$  shown in figure 3.1a. The corresponding probability distribution of one of the zero-energy states can be seen in figure 3.1b. This state is one of the *Majorana states* that formed around the vortex. Upon close inspection of the corners and edges, one can also see a slight probability accumulation. When investigating the slightly higher energy states above and below the newly formed vortex *Majorana states*, we observe a probability distribution nearly identical to that of the *Majorana states* on the normal square lattice, as shown in figure 2.2b.

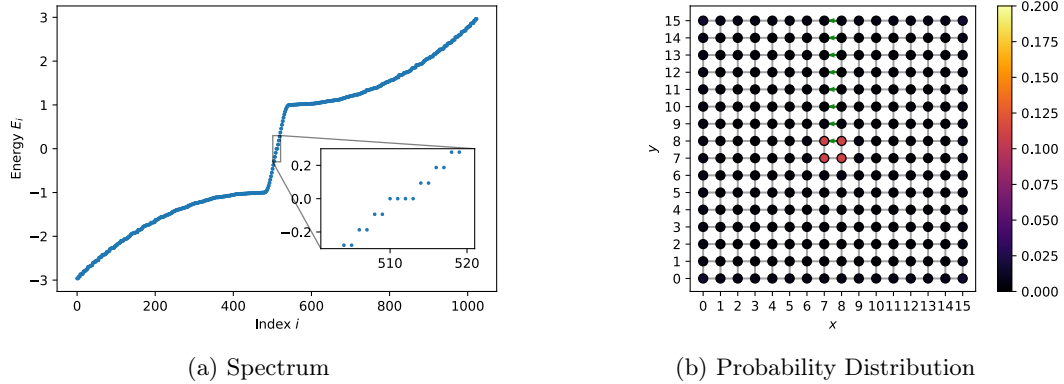


Figure 3.1: Chiral  $p$ -wave superconductivity on a Square Lattice with a  $\pi$ -Vortex

The fact that the edge and vortex *Majorana zero mode* energies are on different scales is rather intriguing. A numerical investigation shown in figure 3.2 highlights the different scaling behaviour of the *Majorana states*. The plots depict the *Majorana zero mode* with the lowest absolute value of Energy  $\min |E_i|/t$  for square lattices of different sizes with and without a vortex as shown in figures 3.1 and 2.2 respectively. Note that figure 3.2a on the left is a log-log plot while figure 3.2b is a lin-log plot. A linear least-squares fit was used to calculate the scaling coefficients of the respective cases.

### 3 Results

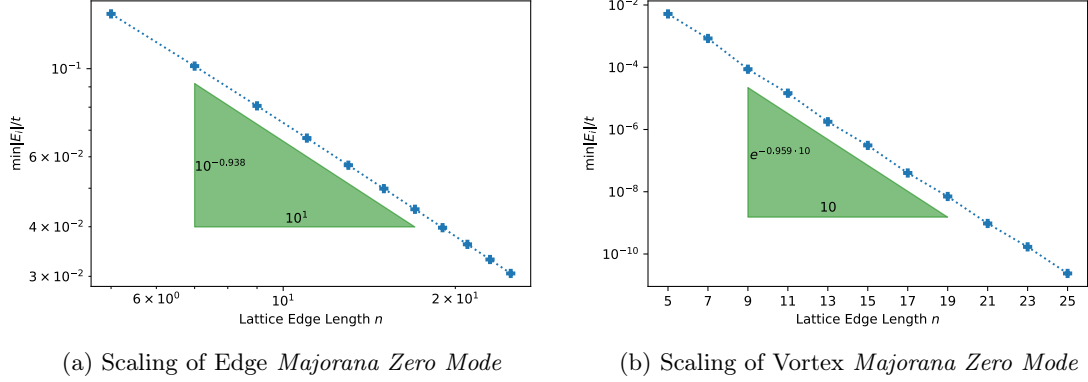


Figure 3.2: Comparison of Edge and Vortex *Majorana zero modes* Energy Scaling for  $n \times n$  Square Lattice

We can conclude that the energy of the *Majorana zero modes* found on the edges and vortices approximately scale as  $E_i \sim n^{-0.94}$  and  $E_i \sim e^{-0.96n}$  respectively. A possible explanation for the exponential decay of the vortex *Majorana zero mode* energy is that the condensate wave-function recovers exponentially characterized by a correlation length  $\xi$ . Due to the finite size of the lattice, the condensate wave-function does not fully recover on the length scale of the lattice. If one analyzes figure 3.1b closely, one can see a slight finite probability in the sites located on the corners.

Conducting further experiments with the parameters and the placement of the vortex phase is consistent with the theoretical framework established so far. For example, if we instead add the  $\pi$ -phase to bonds in the middle of the lattice and also include a phase along bonds in the horizontal direction we get the spectrum and probability distribution of figure 3.3b. We observe multiple vortices; one at each end of the phase-chains. Note that the parameters were changed to  $2\mu/t = \Delta/t = 1$  for this numerical experiment.

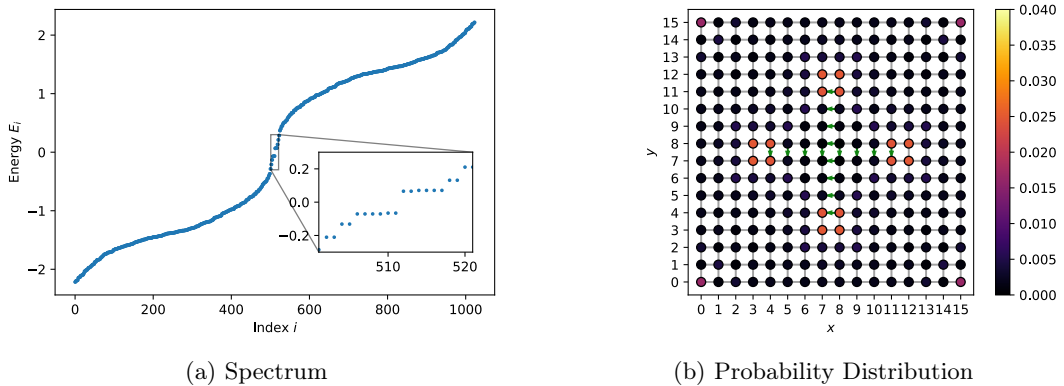


Figure 3.3: Chiral  $p$ -wave superconductivity on Square Lattice with multiple  $\pi$ -Vortices

### 3 Results

## 3.2 Square Lattice with a Single Disclination

In the previous section 3.1 we saw how adding a phase to a string of bonds leads to vortex *Majorana zero modes*. It turns out that the same transformation used to construct vortices 3.6 can be used to account for disclinations. A disclination is a topological defect that *locally* violates a rotational symmetry of the lattice [7]. The square lattice we are currently investigating has four-fold rotational symmetry. We can therefore construct a topological defect by creating a *locally* three-fold symmetric part of the lattice.

The Volterra process is an example of such a construction procedure [7, 18, 19]. It consists of the four different steps shown in figure 3.4. First, a square lattice is initialized. Then the top quadrant is removed from the lattice and bonds are introduced between the newly formed edges such that a three-fold symmetric cell is created in the center of the lattice. A transformation to the coordinates is applied in the final step. Note that the transformation function and code to get from figure 3.4c to figure 3.4d were taken directly from [7] and are only applied to highlight the symmetries of the lattice.

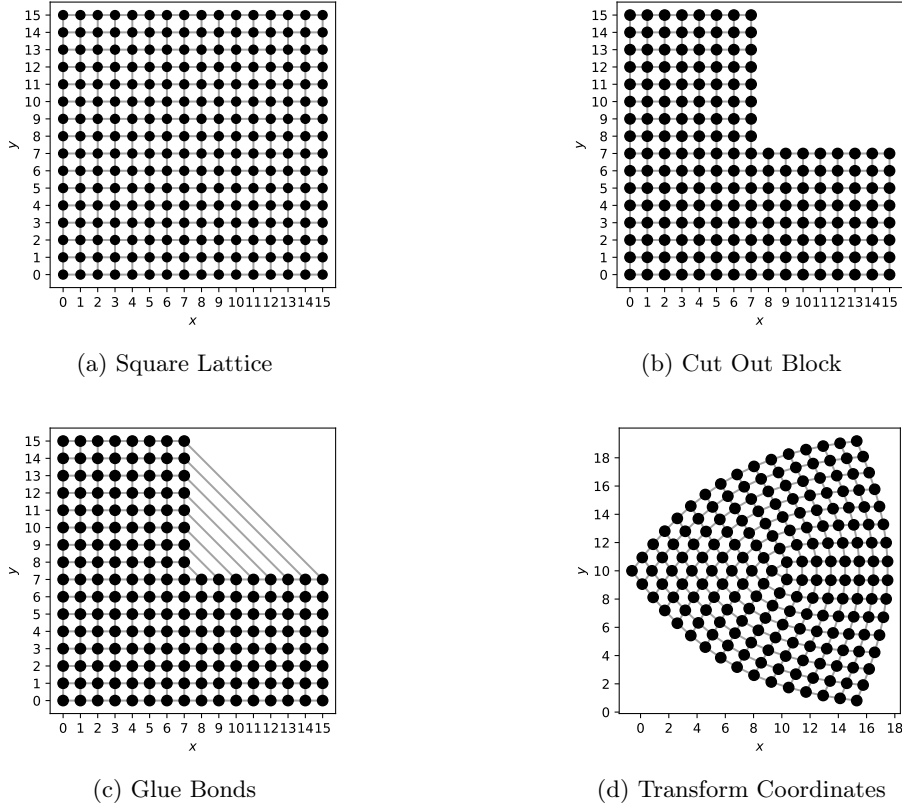


Figure 3.4: Volterra Process Implementation

By introducing a disclination with three-fold symmetry in the center of our lattice we must add a geometric phase  $\phi_g$  corresponding to the so-called Frank angle of  $\pi/2$  [7].

### 3 Results

Intuitively, this phase can be understood as compensating for the missing corner of a triangle compared to a square. As opposed to the vortex phase, it was numerically observed that the geometric phase needs to be applied to the bonds perpendicular to the bonds involved in glueing the lattice together shown in figure 3.4c. Additionally, we must make sure that any closed path around the disclination always picks up the geometric phase. After applying the geometric phase we would expect to see edge *Majorana zero modes*. In figure 3.5b we can observe this predicted behaviour.

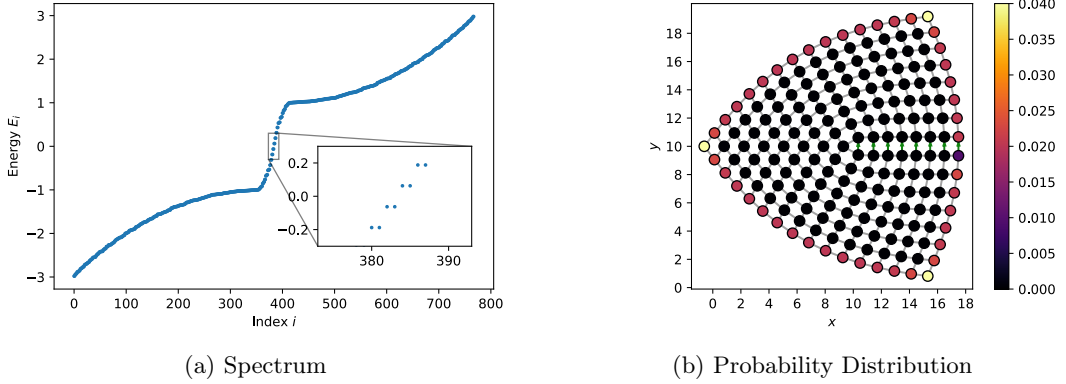


Figure 3.5: Chiral  $p$ -wave superconductivity on Square Lattice with Disclination

If we now add an additional vortex phase such that the vortex is centred at the disclination we get the spectrum and probability distribution shown in figure 3.6. In this case, we applied both phases to the same bonds, however, we could have applied the vortex phase to different bonds so long as any closed path around the disclination would pick up the phase.

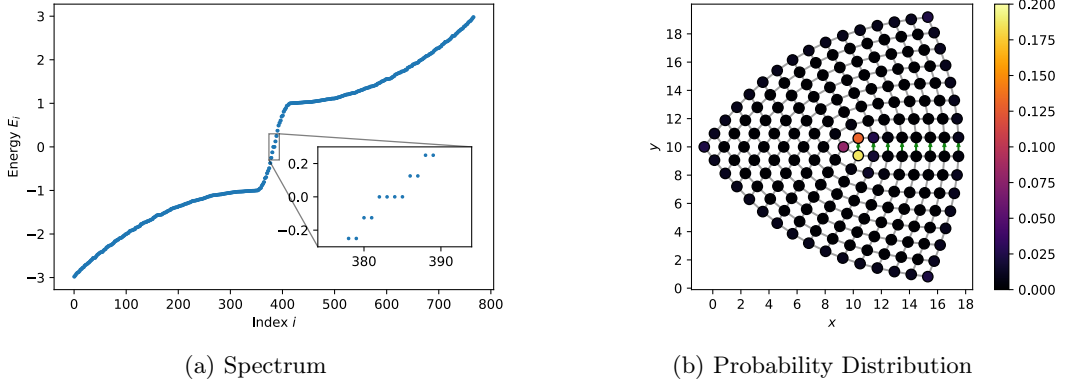


Figure 3.6: Chiral  $p$ -wave superconductivity on Square Lattice with Disclination and Vortex

### 3 Results

#### 3.3 Square Lattice with Disclination Dipole

So far we have analyzed a single disclination in a lattice. This is equivalent to a single magnetic flux [3]. We now move on to the dipole equivalent by introducing an additional disclination with the opposite geometric phase, namely  $\phi_g = -\pi/2$ . We do this by using a Volterra process that creates two separate local parts of the lattice with three-fold and five-fold rotational symmetry.

The Volterra process outlined in [7] is depicted in figure 3.7. First, a square portion of the lattice is removed. In addition to this, bonds near the top right corner are removed. Now we can create the part of the lattice with local three-fold symmetry by glueing the right and bottom edge of the inner square together as shown in figure 3.7c.

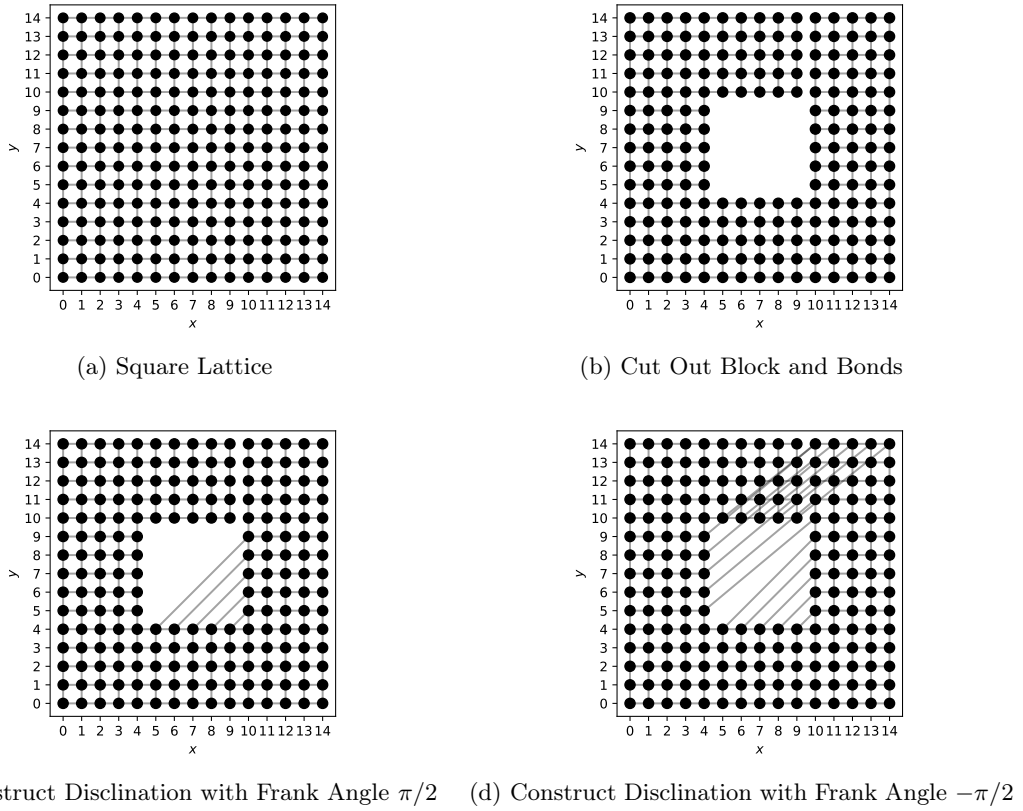


Figure 3.7: Volterra Process Implementation for Disclination Dipole [7]

The local five-fold rotational symmetry is introduced by connecting the remaining sites as shown in figure 3.7d. We once again have to add a phase to the bonds in the lattice such that any closed path around the three-fold and five-fold rotationally symmetric defects pick up a phase of  $\pi/2$  and  $-\pi/2$  respectively. This was achieved by adding the geometric phase  $\phi_g = \pi/2$  to the bonds in-between the triangle- and pentagon-shaped disclinations as can be seen in figure 3.8b.

### 3 Results

Once again we observe *Majorana states* with their support located primarily along the edges of the lattice. The phase was chosen such that a closed path in the mathematically positive direction around the triangular disclination picks up a  $\pi/2$ -phase.

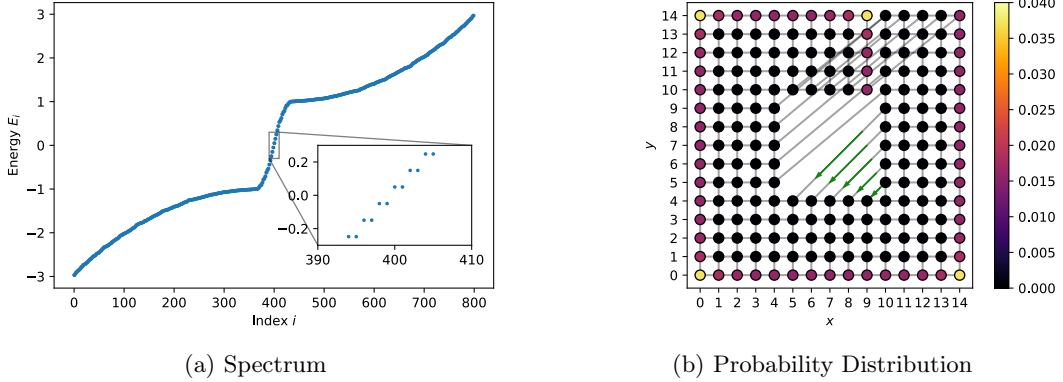


Figure 3.8: Chiral  $p$ -wave Superconductivity on Disclination Dipole

If we add an additional vortex phase of  $\phi_v = \pi$  along the same bonds we observe vortex *Majorana states* around the two topological defects as seen in figure 3.9b.

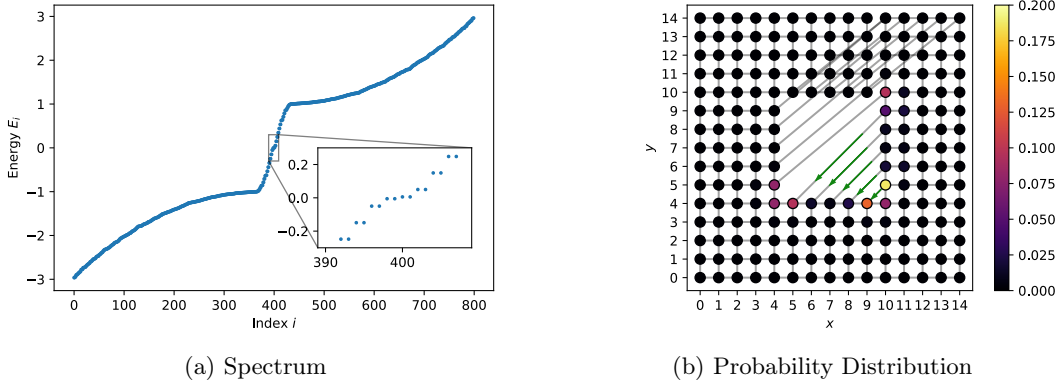


Figure 3.9: Chiral  $p$ -wave Superconductivity Disclination Dipole and Two Vortices

### 3.4 Numerical Implementation

The superconductivity simulations were implemented in PYTHON using the NUMPY and SCIPY package. A lattice is represented as an undirected graph, in a format that is similar to an adjacency list, where a vertex represents a lattice point and an edge represents a bond between two sites. The code<sup>i</sup> is written to be as general as possible and largely resembles the KWANT [20] package in terms of structure. The numerical experiments regarding the single disclination in figures 3.5 and 3.6 were also implemented in KWANT by adapting the source code from [7] after the package and source code were discovered toward the end of the project.

Assembling the real-space Hamiltonian  $H_r$  from equation 2.14 is handled by a constructor class. This class is also used to apply the geometric and vortex phases to bonds. The code for the coordinate transformation used in figure 3.7d was taken and adapted from the source code found in [7].

---

<sup>i</sup>GITHUB link: <https://github.com/isschoch/chiral-p-wave-on-buckyball-geometry>

# Conclusion

---

## 4.1 Summary of the Project

A theoretical framework for the simulation of chiral  $p$ -wave superconductivity was outlined in chapter 2. In addition, simulations on defect-free lattices, the results of which were consistent with theoretical predictions, were performed. Chapter 3 started with an introduction to vortices which were then later placed at the center of disclinations. Furthermore, the convergence of the energy associated with vortex and edge *Majorana zero modes* was investigated. It was found that both energies converge, albeit at different rates: The former energy converges exponentially with the edge length while the latter energy only converges inversely with it.

To perform a simulation on a lattice with a disclination dipole, the Volterra process was outlined and performed on a square lattice. The simulation results were in-line with the theoretical predictions.

## 4.2 Outlook

In order to achieve a simulation on a Buckyball geometry, a disclination simulation with Frank angle  $\pi/3$  should be performed on a honeycomb lattice. The first steps to performing such a simulation have been implemented in the lattice class used thus far. Once this is completed, a Buckyball lattice must be constructed. The pentagon-shaped faces can be handled as disclinations in the lattice.

# Bibliography

1. Meissner, W. & Ochsenfeld, R. Ein neuer Effekt bei Eintritt der Supraleitfähigkeit. *Naturwissenschaften* **21**, 787–788. ISSN: 1432-1904. <https://doi.org/10.1007/BF01504252> (Nov. 1933).
2. Thuneberg, E. in *Encyclopedia of Condensed Matter Physics* (eds Bassani, F., Liedl, G. L. & Wyder, P.) 128–133 (Elsevier, Oxford, 2005). ISBN: 978-0-12-369401-0. <https://www.sciencedirect.com/science/article/pii/B0123694019007105>.
3. Volovik, G. Monopoles and fractional vortices in chiral superconductors. *Proceedings of the National Academy of Sciences of the United States of America* **97**, 2431–6 (Apr. 2000).
4. Kvorning, T., Hansson, T. H., Quelle, A. & Smith, C. M. Proposed Spontaneous Generation of Magnetic Fields by Curved Layers of a Chiral Superconductor. *Phys. Rev. Lett.* **120**, 217002. <https://link.aps.org/doi/10.1103/PhysRevLett.120.217002> (21 May 2018).
5. Commons, W. *File:Buckminsterfullerene-perspective-3D-balls.png* — Wikimedia Commons, the free media repository [Online; accessed 25-April-2022]. 2020. <https://commons.wikimedia.org/w/index.php?title=File:Buckminsterfullerene-perspective-3D-balls.png&oldid=467374384>.
6. Volovik, G. E. Fermion zero modes on vortices in chiral superconductors. *JETP Lett.* **70**, 609–614. arXiv: [cond-mat/9909426](https://arxiv.org/abs/cond-mat/9909426) (1999).
7. Geier, M., Fulga, I. & Lau, A. Bulk-boundary-defect correspondence at disclinations in rotation-symmetric topological insulators and superconductors. English. *SciPost Physics* **10**. ISSN: 2542-4653 (2021).
8. Nayak, C., Simon, S. H., Stern, A., Freedman, M. & Das Sarma, S. Non-Abelian anyons and topological quantum computation. *Rev. Mod. Phys.* **80**, 1083–1159. <https://link.aps.org/doi/10.1103/RevModPhys.80.1083> (3 Sept. 2008).
9. Powell, B. Introduction to Effective Low-Energy Hamiltonians in Condensed Matter Physics and Chemistry. *Computational Methods for Large Systems: Electronic Structure Approaches for Biotechnology and Nanotechnology* (June 2009).

## Bibliography

10. Sigrist, M. *Lecture Notes: Superconductivity* 2020. <http://www.vvz.ethz.ch/lerneinheitPre.do?semkez=2020W&lerneinheitId=140328&lang=en>.
11. Neupert, T. *Lecture Notes: Introduction to Condensed Matter Physics* 2019.
12. Huber, S. & Neupert, T. *Lecture Notes: Topological Condensed Matter Physics* 2021. <http://www.vvz.ethz.ch/lerneinheitPre.do?semkez=2021S&lerneinheitId=153001&lang=en>.
13. Kitaev, A. Y. Unpaired Majorana fermions in quantum wires. *Physics-Uspekhi* **44**, 131–136. <https://doi.org/10.1070/1063-7869/44/10s/s29> (Oct. 2001).
14. Ryu, S. & Hatsugai, Y. Topological Origin of Zero-Energy Edge States in Particle-Hole Symmetric Systems. *Phys. Rev. Lett.* **89**, 077002. <https://link.aps.org/doi/10.1103/PhysRevLett.89.077002> (7 July 2002).
15. Leijnse, M. & Flensberg, K. Introduction to topological superconductivity and Majorana fermions. *Semiconductor Science and Technology* **27** (June 2012).
16. Ryu, S., Schnyder, A. P., Furusaki, A. & Ludwig, A. W. W. Topological insulators and superconductors: tenfold way and dimensional hierarchy. *New Journal of Physics* **12**, 065010. <https://doi.org/10.1088/1367-2630/12/6/065010> (June 2010).
17. Sigrist, M. *Lecture Notes: Statistical Physics* 2021. <http://www.vvz.ethz.ch/lerneinheitPre.do?semkez=2021W&lerneinheitId=147094&lang=en>.
18. Varjas, D. *et al.* Topological Phases without Crystalline Counterparts. *Phys. Rev. Lett.* **123**, 196401. <https://link.aps.org/doi/10.1103/PhysRevLett.123.196401> (19 Nov. 2019).
19. Volterra, V. Sur l'équilibre des corps élastiques multiplement connexes. fr. *Annales scientifiques de l'École Normale Supérieure* **3e série**, **24**, 401–517. <http://www.numdam.org/articles/10.24033/asens.583/> (1907).
20. Groth, C. W., Wimmer, M., Akhmerov, a. R. & Waintal, X. Kwant : a software package for quantum transport. *New Journal of Physics* **16**, 63065. <https://hal-cea.archives-ouvertes.fr/cea-01089977> (2014).